remote sensing

MDPI

Article

Geophysical and Remote Sensing Assessment of Chad's Groundwater Resources

Ahmed Mohamed [1], Ahmed Abdelrady [2,*], Saad S. Alarifi [3] and Abdullah Othman [4]

[1] Geology Department, Faculty of Science, Assiut University, Assiut 71516, Egypt
[2] Faculty of Civil Engineering and Geoscience, Delft University of Technology, 2629 HS Delft, The Netherlands
[3] Department of Geology and Geophysics, College of Science, King Saud University, P.O. Box 2455, Riyadh 11451, Saudi Arabia
[4] Department of Environmental Engineering, Umm Al-Qura University, Makkah 24382, Saudi Arabia
* Correspondence: a.r.a.mahmoud@tudelft.nl

Abstract: Because of climate change and human activity, North and Central Africa are experiencing a significant water shortage. Recent advancements in earth observation technologies have made widespread groundwater monitoring possible. To examine spatial and temporal mass fluctuations caused by groundwater variations in Chad, gravity solutions from the Gravity Recovery and Climate Experiment (GRACE), climatic model outputs, and precipitation data are integrated. The results are as follows: (1) The investigated region experienced average annual precipitation (AAP) rates of 351.6, 336.22, and 377.8 mm yr^{-1}, throughout the overall investigation period (04/2002–12/2021), Period I (04/2002–12/2011), and Period II (01/2012–12/2021), respectively. (2) Using the three gravity solutions, the average Terrestrial Water Storage Variations (ΔTWS) values are estimated to be +0.26 ± 0.04, +0.006 ± 0.10, and +0.64 ± 0.12 cm yr^{-1}, for the overall study period, periods I, and II, respectively. (3) Throughout the full period, periods I, and II, the groundwater storage fluctuations (ΔGWS) are calculated to be +0.25 ± 0.04, +0.0001 ± 0.099, and +0.62 ± 0.12 cm yr^{-1}, respectively after removing the soil moisture (ΔSMS) and Lake Chad water level trend values. (4) The country receives an average natural recharge rate of +0.32 ± 0.04, +0.068 ± 0.099, and +0.69 ± 0.12 cm yr^{-1}, throughout the whole period, Periods I, and II, respectively. (5) The southern mountainous regions of Erdi, Ennedi, Tibesti, and Darfur are receiving higher rainfall rates that may recharge the northern part of Chad through the stream networks; in addition to the Lake Chad and the higher rainfall over southern Chad might help recharge the central and southern parts of the country. (6) A preferred groundwater flow path from the Kufra (Chad and Libya) to the Dakhla basin (Egypt) appears to be the Pelusium mega shear system, which trends north-east. The findings suggest that GRACE is useful for monitoring changes in groundwater storage and recharge rates across large areas. Our observation-based methodology provides a unique understanding of monthly ground-water patterns at the state level, which is essential for successful interstate resource allocation, future development, and policy initiatives, as well as having broad scientific implications for arid and semiarid countries.

Keywords: geophysics; time-variable gravity data; terrestrial water storage; groundwater resources; recharge; Chad

Citation: Mohamed, A.; Abdelrady, A.; Alarifi, S.S.; Othman, A. Geophysical and Remote Sensing Assessment of Chad's Groundwater Resources. *Remote Sens.* **2023**, *15*, 560. https://doi.org/10.3390/rs15030560

Academic Editors: Jolanta Nastula and Monika Birylo

Received: 7 December 2022
Revised: 1 January 2023
Accepted: 10 January 2023
Published: 17 January 2023

1. Introduction

Terrestrial water storage (TWS), which is calculated as the sum of water stored in groundwater storage (GWS), soil, rivers, lakes, and dams, and snow as well as in vegetation, is a significant factor in the processes of the land-atmosphere interaction and the global hydrological cycle [1,2]. TWS changes play a significant role in regulating water flux interactions within various Earth system components as they serve as an effective indicator of regional water balance or imbalance [3], ice sheets and glaciers mass fluctuations [4], natural hazards like floods and droughts [5], and sea-level rise [6].

The demand for groundwater, a precious resource, is rising globally. Approximately 98% of the world's liquid freshwater resources are located in groundwater, making it a vital resource for supplying a wide range of water demands (both natural and anthropogenic) and enabling substantial growth in the world's social, agricultural, and industrial sectors [2,5,7]. Due to population increase, overuse, and climate change, more areas around the world are experiencing water scarcity and stress, particularly in dry and semiarid areas. Therefore, a more accurate monitoring system is essential to comprehending the groundwater flow dynamics and developing long-term plans for water management [8].

As the major supply of water for more than half of the world's population, or 2 billion individuals, groundwater is a vital resource. In fact, it is estimated that between 40 and 50 percent of the world's food supply is irrigated using groundwater. Groundwater consumption varies widely around the world, depending on factors such as local climate and water infrastructure. In dry, arid locations, where alternative supplies of water are limited, groundwater is of prime significance. Several issues can put a strain on our groundwater supplies, but one of the most serious is groundwater depletion. In example, withdrawals in dry and semi-arid areas, where people rely on groundwater for agricultural and home purposes can rapidly exceed net recharge [9,10]. Even in developed countries, the laws protecting groundwater rights have not changed in response to the increasing demands on water resources placed on by population increase and economic development [10].

A lack of groundwater data can complicate resource management [11–13]. This is especially true when looking at the longer time intervals necessary to assess aquifer sustainability [14]. Setting up a network of monitoring wells and regularly collecting, storing, and analyzing water level and quality data over lengthy intervals requires a lot of effort and resources [14]. Poor management of aquifers is frequently due to a lack of information and knowledge of the consequences of groundwater depletion [10,15,16]. Moreover, data collecting is hampered in many regions of the world by the scarcity of field observation gauges globally, gaps in time, and limited data exchange because of societal and political constraints, and the significant uncertainties in hydrological and land surface models. Therefore, global variations in TWS and GWS are still not fully understood [2,8,17].

Using satellite data for remotely sensed monitoring could be a solution for these restrictions. In addition, remote sensing typically provides open datasets that can be used to better track hydrological variations in inaccessible regions. However, continuous time series data is necessary for comprehending temporal patterns of hydrological changes in a particular location and time.

Conventional methods such as physical, chemical, and modeling techniques have been evaluated the depletion and recharge rates of significant hydrogeological settings, including aquifer systems [18–21]. However, these procedures are difficult to utilize on a regional scale, and their findings are sometimes disputed, because of a paucity of datasets required for execution and the time and money needed to collect them.

There have been about two decades since the first launch of GRACE, and therefore we have numerous studies employing similar methodologies. For rainfall and surface water studies, remote sensing applications were more actively utilized for locations with a lack of data. For the Tanzania's Rufiji Basin, [22] evaluated the viability of water budget predictions from Gravity Recovery and Climate Experiment (GRACE), and Tropical Rainfall Measuring Mission (TRMM) data with other relevant images. When compared to previous research in the same basin, estimates of rain, evaporation, and water storage were found to be more precise in the study.

Ref. [23] used the time series from the Global Inundation Extent from Multi-Satellites, TRMM, GRACE, and ENVISAT radar altimeter to estimate the storage and extent of surface water in the basin of the Congo River. They concluded that the Ubangi, Lualaba, and Sangha basins, among others, accounted for a sizable share of the total water storage change that occurred in the subsurface. Their study defined the term "subsurface water storage" as the sum of groundwater (GWS) and soil moisture storages (SMS).

Ref. [8] examined the validity of the ΔGWS assessed by GRACE in context with limited information for the Ngadda watershed in the Basin of the Lake Chad. Their study demonstrated that, despite the limitations of modeling and lack of available in-situ data, GRACE-based estimation for ΔGWS might be a practical and affordable alternative technique to monitor how groundwater changes at a basin size.

Key seasonal components of the continental water cycle were globally described using the monthly data in the early stages of GRACE application development [24–26]. Recently, droughts, evapotranspiration, ice mass variations, and surface runoff during flooding events have considered as hydrological components that can be defined using GRACE's integral signals [27,28]. Applications for the change in groundwater capacity have been made for a wide variety of hydrologic settings and sizes [10,29–42].

Contributions from different ΔTWS compartments cannot be distinguished by GRACE such as surface water (ΔSWS), canopy water (ΔCWS), soil moisture (ΔSMS), snow water equivalent (ΔSWE), groundwater storage (ΔGWS). This problem was solved by integrating outputs of the climatic model with GRACE data, which enabled the separation of different parts from GRACE-extracted TWS estimations and an increase in the horizontal resolution of the data [43]. To simulate the interplay of the land surface, atmosphere, oceans, and ice, among other significant climate drivers, climate model outputs use quantitative methods. These models have numerous uses in the management of water resources, water cycle modeling, and climate prediction. The Global Land Data Assimilation System (GLDAS; [10,44,45]) is one of them. GLDAS gathers observational data from ground and orbiting platforms. Using advanced land surface simulation and data assimilation methods, it determines the ideal fields of land surface states and fluxes.

Recent statistics show that only around 20% of Chad's groundwater withdrawal is used for human consumption, while the remaining 80% is used in agriculture [46]. Water for human use and, in certain cases, cattle consumption during dry seasons is a necessity in many rural communities, especially in the drier northern parts, and this water must come from shallow hand-dug wells and boreholes. Local irrigation in the northern region frequently employs groundwater. Many large cities, including N'Djamena, rely heavily on groundwater for their municipal water supply [47]. Infrequent industrial uses of groundwater extraction include textile manufacturing, sugar processing, cotton milling, and beer brewing. In order to effectively manage groundwater in Chad, it is important to have an understanding of how the groundwater supplies tend to fluctuate over time.

In addition to GRACE's applications, other recent global fields, such as Gravitational Models of the Earth, which provide gravity fields, have been used to examine crustal structures and properties on a global scale [48]. Small-scale applications of geophysical data collected from aircraft and/or the ground have also been utilized to study groundwater, subsurface geology, mineralization zones [49,50], the structure of the magma chamber [51], and land subsidence [52].

Three GRACE mascon (mass concentration block) products are integrated with GLDAS outputs to estimate and analyze spatio-temporal variations of ΔTWS and to estimate the groundwater storage anomalies, the recharge, and/or depletion rates caused by climatic effects and/or anthropogenic activities in the Republic of Chad. We also investigated how the TRMM-derived rainfall rate affects the variations in groundwater storage and the groundwater flow.

2. Study Area

At the confluence of North and Central Africa, the landlocked republic of Chad is located. To the north, it shares borders with Libya; Sudan, from the east; Central African Republic from the south; to the southwest, Cameroon and Nigeria (near Lake Chad); and to the west, Niger. Chad has several climatic zones varying from a fertile Sudanian Savanna zone in the south, an arid Sahleian belt in the center, to a desert zone in the north. The country of Chad gets its name from the second-largest wetland in Africa, Lake Chad.

The geology of study area is represented by sediments from the Precambrian and more recent eras that surround the central Chad Basin. The Tibesti Mountains in the country contain Precambrian rocks. The Nubian sandstones are deposited on top of Lower Paleozoic sandstone strata in the northeastern Kufra Basin. While marine deposits are present in the Upper Cretaceous. Continental clastic rocks make up the Lower Cretaceous. Parts of southern Chad are covered with Tertiary continental deposits. Lacustrine sediments make up the Neogene Chad Formation throughout most of the Chad Basin.

The Tibesti highlands, home to some of the Sahara's highest peaks, are found along the country's border with Libya (Figure 1). The highest summits are Cenozoic volcanoes, some of which directly overlie the crystalline rocks, which are frequently entirely encircled and layered with sediments from below. A significant portion of the sedimentary cover is composed of Cambrian to Ordovician continental sandstones that overlies with obvious unconformity the Precambrian rocks in northern Chad, particularly on the eastern, southern, and western flanks (Figure 1).

Eastern Chad has a significant amount of exposed basement rocks that cross the Sudanese border into the Darfur Province. Granitic gneisses, quartzo-feldspathic, pelitic, and graphitic schists are the most common rock types, whereas volcanic and calcareous rocks are less common. Many of the rocks are in the regional metamorphism grade of amphibolite, and the folding is typically on northeast axes. The schists and gneisses are broken by several late-orogenic granitic batholiths, where pegmatites and quartz veins have developed in some locations and tin and wolfram mineralization has taken place. Ages between 590 and 570 Ma have been obtained from intrusive granitoids.

The Kufra Basin spans NE Chad, NW Sudan, and SE Libya and has a NE-to-SW direction. The Kufra Basin is one of the nearby intracratonic basins in North Africa with a comparable sedimentological and geological history. Together, they constitute a large Palaeozoic mega province with both significant current output and significant unrealized potential. It is made up of a sequence of Paleozoic rocks dating from the Cambrian to the Carboniferous periods.

The Chad Basin is a collection of buried rifts with an NW-SE trend that is situated in the western part of central Chad and southeast Niger. These submerged rifts are covered with Quaternary sand dunes. The series, which can be up to 4000 m deep, starts with "Continental Intercalaire" Group Permo-Triassic to Early Cretaceous fluviatile and lacustrine non-marine strata. These strata are then covered by Cenomanian-Coniacian carbonates and marine shales. Gypsiferous, glauconitic, and fossiliferous shales from the Upper Cretaceous, which extends into the Santonian and Campanian, continue to record marine influence. The "Continental Terminal" is made up of Tertiary non-marine beds that rest irregularly over Maastrichtian-Paleocene continental sandstones with oolitic iron stones.

Figure 2 shows the aquifer types and productivity in Chad. The Lake Chad Basin is one of the continent's major sedimentary groundwater basins in southern Chad [47]. It consists of three major aquifers: (1) an unconsolidated aquifer with lacustrine and deltaic deposits from the Quaternary and Pliocene (the Chad Formation) that is dominated by permeable sands of high productivity. Its upper portion is often unconfined and semi-confined/confined by clay layers [53], and its shallowest zone is hydraulically connected to Lake Chad and the Logone-Chari river system. Clay strata constrain parts of the lower aquifer; (2) a Tertiary sequence under this (the Continental Terminal Formation) of moderate to high productivity, it is represented by alternating sandstone and clay-rich bands of the Continental Terminal that lie beneath the Pliocene-Quaternary Chad Formation; together they form the Lake Chad Basin Aquifer; and (3) a lower Cretaceous aquifer that is less well understood, it occurs at depth in the Lake Chad Basin in southern and central Chad. In contrast to the Lake Chad Basin, other aquifers in Chad have received less attention and scientific investigation. These aquifers include Precambrian basement rocks, Quaternary valley alluvium, smaller areas of volcanic rocks of low to moderate productivity, other unconsolidated sediments, and Palaeozoic sedimentary rocks in the north that are part of the Nubian Sandstone Aquifer System (NSAS) in the Kufra Basin with moderate to high

productivity, consisting of well-cemented sandstones intercalated with shales and clays. The majority of groundwater flow occurs through fractures within the NSAS [47].

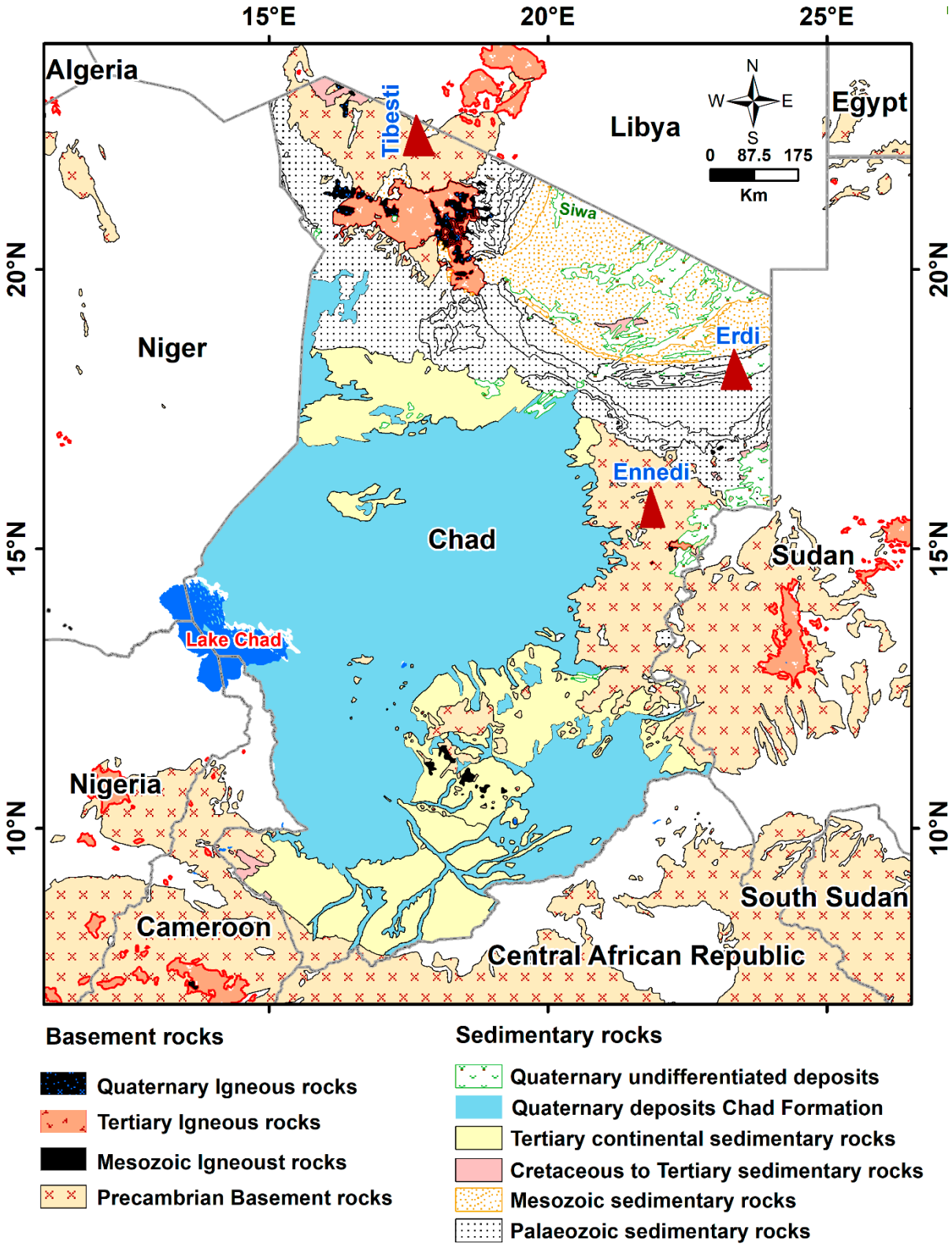

Figure 1. A geological map of the research area.

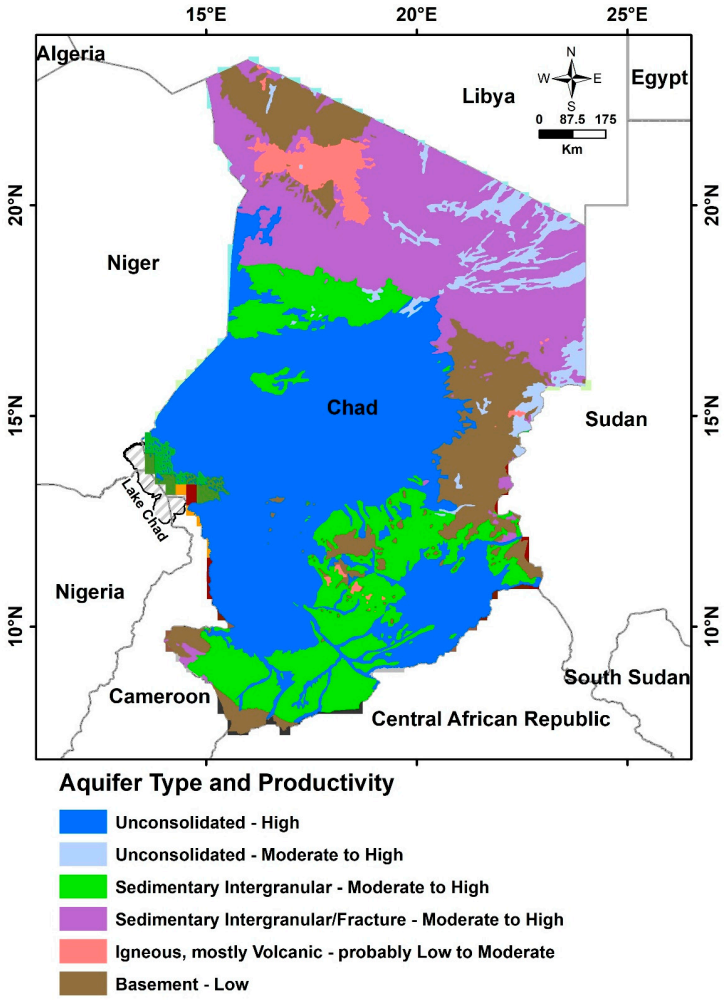

Figure 2. Aquifer type and productivity of the study area.

3. Data and Methods

3.1. Gravity Data

The current investigation utilized three monthly time-varying gravity mascon solutions from GRACE processing centers. The datasets are CSR-RL06M, JPL-RL06M, and GSFC-RL06M, which are provided by CSR, JPL, and NASA Goddard Space Flight Center (GSFC), respectively. Compared to spherical harmonic solutions, these mascon solutions have a higher spatial resolution and less inaccuracy, so they catch all the signals observed by GRACE, while remaining below the GRACE noise thresholds. The use of smoothing and de-striping techniques is unnecessary as some products don't even need the scaling factor [54–57].

In the JPL-RL06M solution, the TWS anomalies were computed for each perfectly balanced 3° × 3° spherical cap mascon block. This solution was released from the Jet Propulsion Laboratory [55,56]: http://grace.jpl.nasa.gov, accessed on 7 December 2022). The final dataset shows TWS fluctuations are on latitude and longitude grids of 0.5° on each side. Given that, the JPL-RL06M has a spatial resolution of 3°, thus the leakage signals caused by 3° mascon blocks were recovered according to JPL-provided scaling factors. JPL-RL06 data, as opposed to the earlier version (JPL-RL05M), clearly distinguish between land and ocean mascons.

In the CSR-RL06M solution, the TWS anomalies are shown in the 0.25° square grids that were computed from a region with a 1° spatial resolution. This solution was released from the Center for Space Research [57,58]: http://www2.csr.utexas.edu/grace/, accessed on 7 December 2022). The hexagonal coastal tiles in this new grid are splitted into ocean

and land blocks to lessen leakage errors between them. For these tiny blocks, there is no need for the scaling factor.

The GSFC-RL06v1.0 mascon solution was employed alongside the CSR and JPL mascon datasets. This solution shows TWS anomalies in 0.5° equal-area square mascons. It was released by NASA GSFC [59]: https://earth.gsfc.nasa.gov/geo/data/grace-mascons, accessed on 7 December 2022).

We have employed the mean of the JPL-RL06M, CSR-RL06, and GSFC-RL06 to conduct this study, which covered the period from April 2002 to December 2021. The noise in the gravity field solutions was found to be effectively reduced using the ensemble mean of the CSR, JPL, and GFZ solutions [60].

Interpolating the missing data was done using the cubic-spline technique. The slope values of ΔTWS trends were determined. The associated errors with the estimated trend values were then computed.

3.2. GLDAS

To estimate the ΔGWS change, outputs of GLDAS should be used with GRACE data. This estimates the non-groundwater parts that must be removed from the GARCE-estimated ΔTWS change using the following Equation (1); e.g., [10,61,62]:

$$\Delta GWS = \Delta TWS - (\Delta SMS + \Delta SWE + \Delta CWS + \Delta SWS) \quad (1)$$

The results of the GLDAS model are used to estimate changes in ΔSMS, ΔSWE, and ΔCWS, while the change in surface reservoir storage (ΔSWS) is estimated from the surface water level series of Lake Chad, taken from the U.S. Department of Foreign Agricultural Service (USDA-FAS), global reservoir, and lake monitoring database [63].

We used the GLDAS datasets [44]: https://disc.gsfc.nasa.gov/datasets?keywords=GLDAS, accessed on 7 December 2022) due to the paucity and unavailability of gauge station datasets in certain places of the study area. Three GLDAS versions (NOAH, VIC, and CLM) were utilized in the current investigation. The data was gathered at the same time as GRACE data every month, but with a 1° spatial resolution.

3.3. Lake Chad Reservoir

Lake Chad (Figure 1) is a large, shallow, and seasonally fluctuating endorheic lake located in the geographic centre of Africa. More than 68 million people who reside in the four nations that surround Lake Chad (Cameroon, Chad, Nigeria, and Niger) on the edge of the Sahara Desert depend on it for their water supply, making it a significant economic resource. The Lake was investigated as a separate water body in the study area. It is anticipated that this water body will have an impact on the GWS estimate over the study area as well as the mass fluctuation inferred from the GRACE data. The trend in the ΔSWS of the lake was determined and subtracted from the TWS change. Using the USDA-FAS datasets, a time record of Lake Chad's surface water level was obtained.

3.4. TRMM

TRMM was created by NASA and the Japanese Space Exploration Agency (NASDA) [64–66]: http://disc.sci.gsfc.nasa.gov/, accessed on 7 December 2022) for the Earth, as a comprehensive, and multidisciplinary research project. It aimed to understand the Earth as a whole and enhance our comprehension of how precipitation is distributed and varies in the tropics as a part of the water cycle in the current climate system. It is intended for use in tropical and subtropical regions to measure rainfall. Most of the inhabited earth was covered by TRMM data, which has a 50°N to 50°S and 180°W to 180°E geographical domain, with a 0.25° × 0.25° spatial resolution. Because there are no available rain gauge stations in Chad, satellite TRMM-based rainfall measurements were utilized to deduce the dominant rainfall patterns over Chad, which reflects the impact of climatic variability on ΔGWS. The monthly TRMM datasets are used to generate the monthly rainfall time series and the average annual precipitation (AAP) rate for the entire study area.

4. Result and Discussion

4.1. Analysis of Rainfall Data

Figures 3 and 4 depict the analysis of TRMM-derived rainfall data. The AAP (Figure 3) shows higher values of 500–1200 mm yr^{-1} at the southern regions of Chad, close to the borders with Cameron and the Central Africa Republic, and decreases northward, reaching lower values of less than 20 mm yr^{-1}, close to the borders with Libya and Niger. The AAP time series displays significantly higher variability, varying from lower values of 270 mm in 2002 to higher values of more than 422 mm during the years 2006, 2012, and 2019 (Figure 4). Two climatic periods can be identified based on the AAP over the study area. Period I (January 2002–December 2011) shows lower AAP rate of 336.22 mm yr^{-1}, whereas period II (January 2012–December 2019) shows higher AAP rate of 377.80 mm yr^{-1}. The AAP rate was estimated to be 351.60 mm during the entire period over the study area (Table 1).

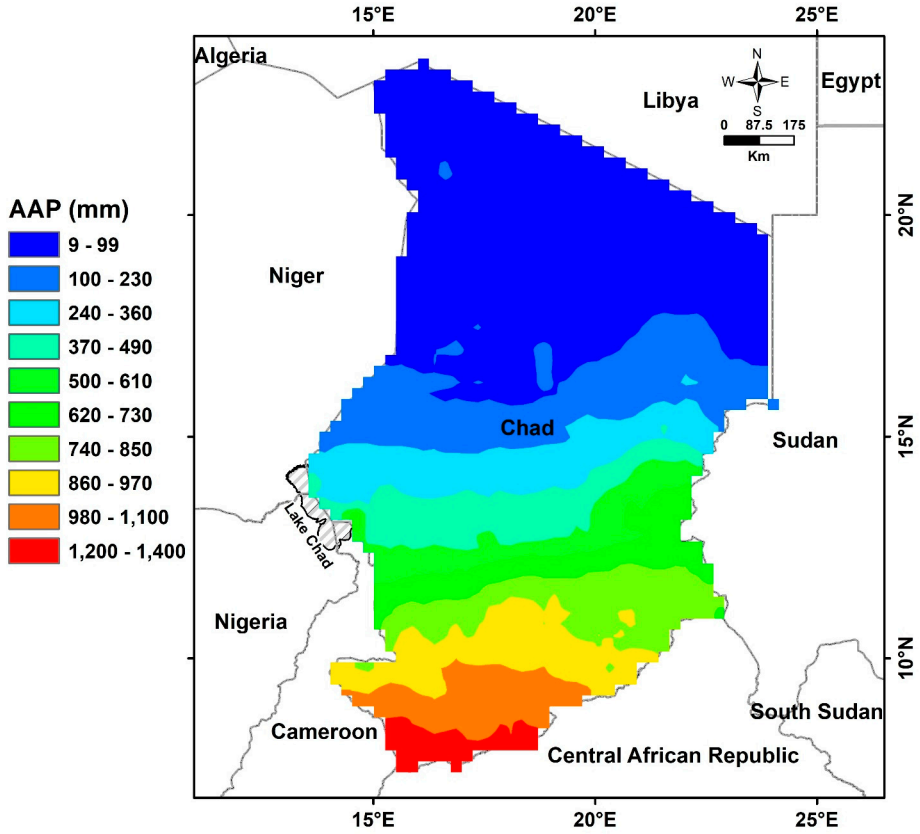

Figure 3. AAP (mm) was extracted from the TRMM data over the study area.

Table 1. Partitioning of terrestrial water storage (ΔTWS) in the study area.

Component		Unit	Whole Period	Period I	Period II
GRACE total (ΔTWS)	CSR	cm yr^{-1}	+0.25 ± 0.04	+0.07 ± 0.10	+0.64 ± 0.12
	JPL		+0.29 ± 0.04	+0.02 ± 0.11	+0.68 ± 0.13
	GSFC		+0.24 ± 0.05	−0.07 ± 0.10	+0.64 ± 0.13
	AVG		+0.26 ± 0.04	+0.006 ± 0.10	+0.64 ± 0.12
ΔSMS		mm yr^{-1}	+0.03 ± 0.02	+0.016 ± 0.133	+0.14 ± 0.013
Lake Chad		mm yr^{-1}	+0.032 ± 0.003	+0.043 ± 0.01	+0.030 ± 0.00
ΔGWS		cm yr^{-1}	+0.25 ± 0.04	+0.0001 ± 0.099	+0.62 ± 0.12
Withdrawal		mm yr^{-1}	−0.68 ± 0.07	−0.68 ± 0.07	−0.69 ± 0.07
Recharge		cm yr^{-1}	+0.32 ± 0.04	+0.068 ± 0.099	+0.69 ± 0.12
AAP		mm	351.6	336.22	377.8

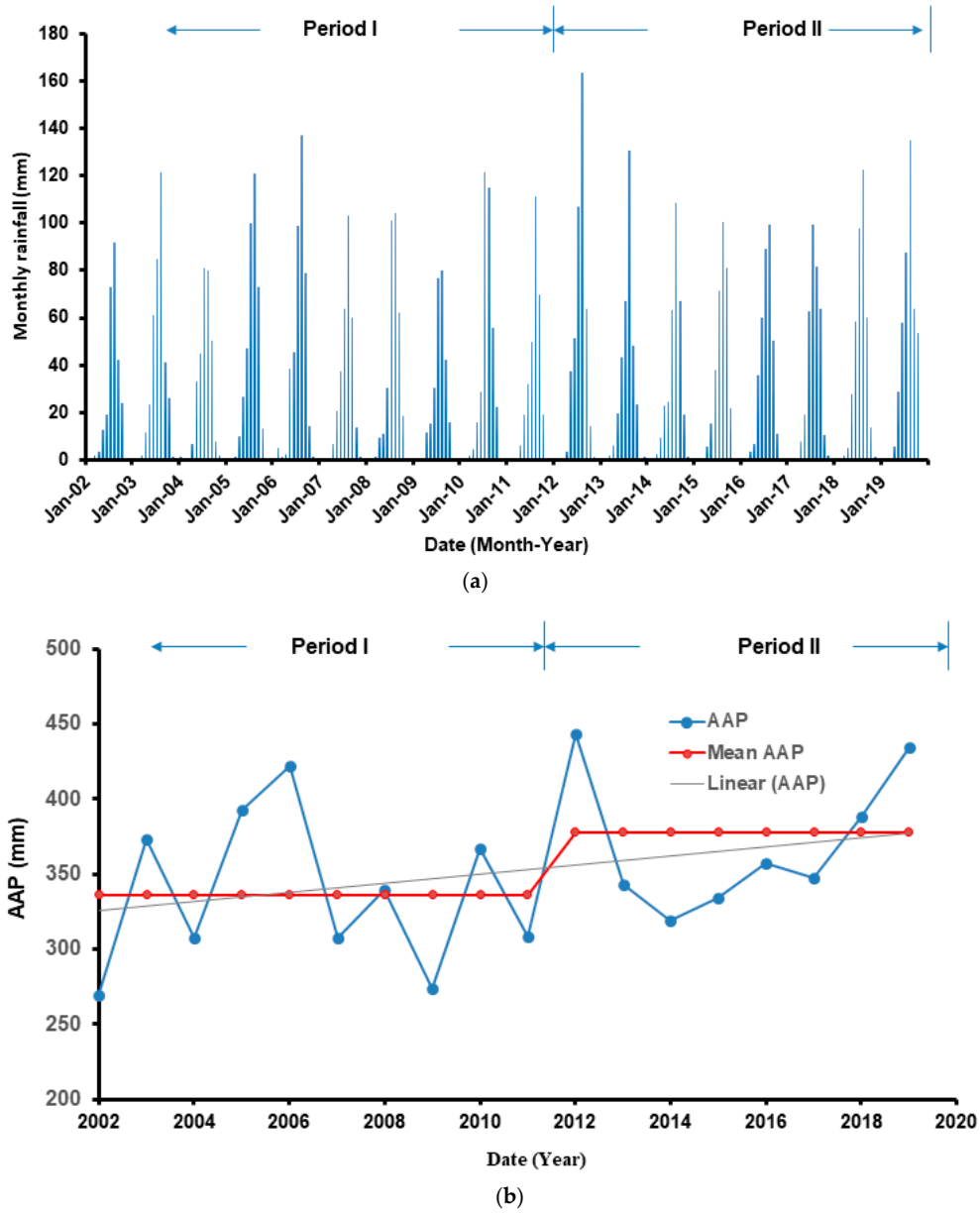

Figure 4. Displays the monthly precipitation (**a**) and annual precipitation (**b**) over the study area for the two periods.

4.2. Analysis of TWS Variations

Figures 5 and 6 show the spatial patterns of the TWS fluctuations across the research region for the two periods. There was a good correlation of 0.97–0.98 between the three TWS time series. Witnessing of Figures 4 and 5 reveals that the northern part is experiencing negative TWS trend values, whereas the southern part is witnessing positive TWS trend values. Figure 7 displays the monthly time series of the averaging TWS changes across Chad, which was obtained by averaging the monthly mascon solutions given by JPL, CSR, and GSFC, as well as the mean of these solutions. Inspection of Figure 7 shows that the different TWS solutions follow a similar pattern. The TWS trends of Period I show lower values compared to those of Period II (Table 1). The TWS estimates of Period I show very slightly depletion to near-steady state rates of $+0.07 \pm 0.10$, $+0.02 \pm 0.11$, and -0.07 ± 0.10 cm yr^{-1}, using the averaging of the mascon CSR, JPL, and GSFC solutions, respectively (Table 1). The three mascon solutions were averaged at $+0.006 \pm 0.10$ cm yr^{-1} for Period I across the entire study area (Figure 7; Table 1). For Period II, the TWS estimates show increasing

trends of +0.64 ± 0.12, +0.68 ± 0.13, and +0.64 ± 0.13 cm yr^{-1} (Table 1), using the averaging of the mascon CSR, JPL, and GSFC solutions, respectively (Table 1). The averaging of the mascon solutions was calculated to be +0.64 ± 0.12 cm yr^{-1} for Period II (Figure 8) across the entire study area. Inspection of Figures 4a and 7 shows that heavy rainfall occurs in May-October and high ΔTWS anomalies occur in August-November/January. Most TWS responses appear to lag behind Chad's rains by about three months. The peak response of GARCE-derived TWS reaction lags rainfall across the Lake Chad region by 1.5 to 2 months, as shown from prior results by [8,67]. The seasonal cycle of TWS in the NW Sahara Aquifer lags behind precipitation by around 2 months and 10 days [68].

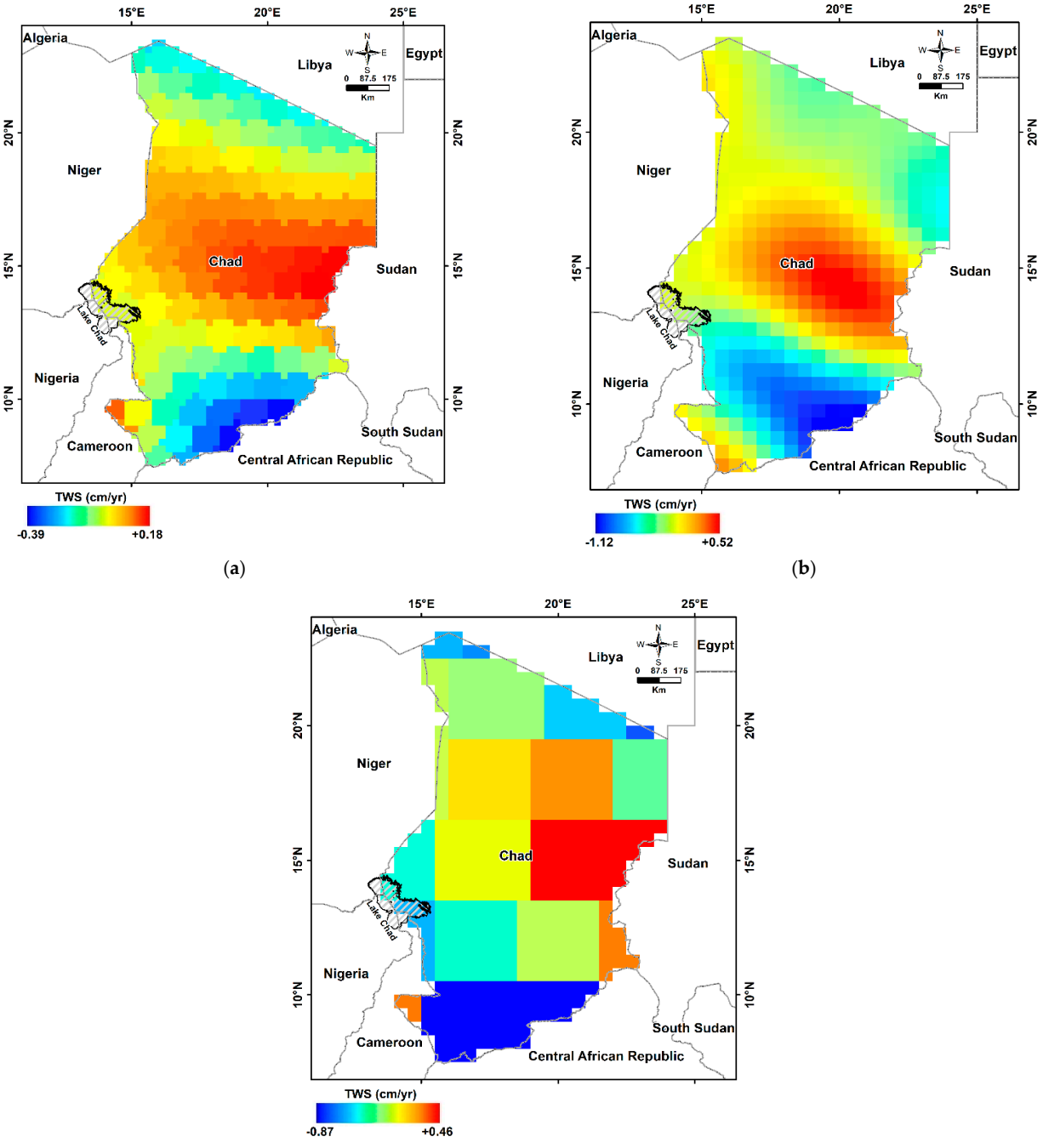

Figure 5. Spatiotemporal variation map of the ΔTWS trend during Period I from CSR (**a**), GSFC (**b**), and JPL (**c**) mascon products.

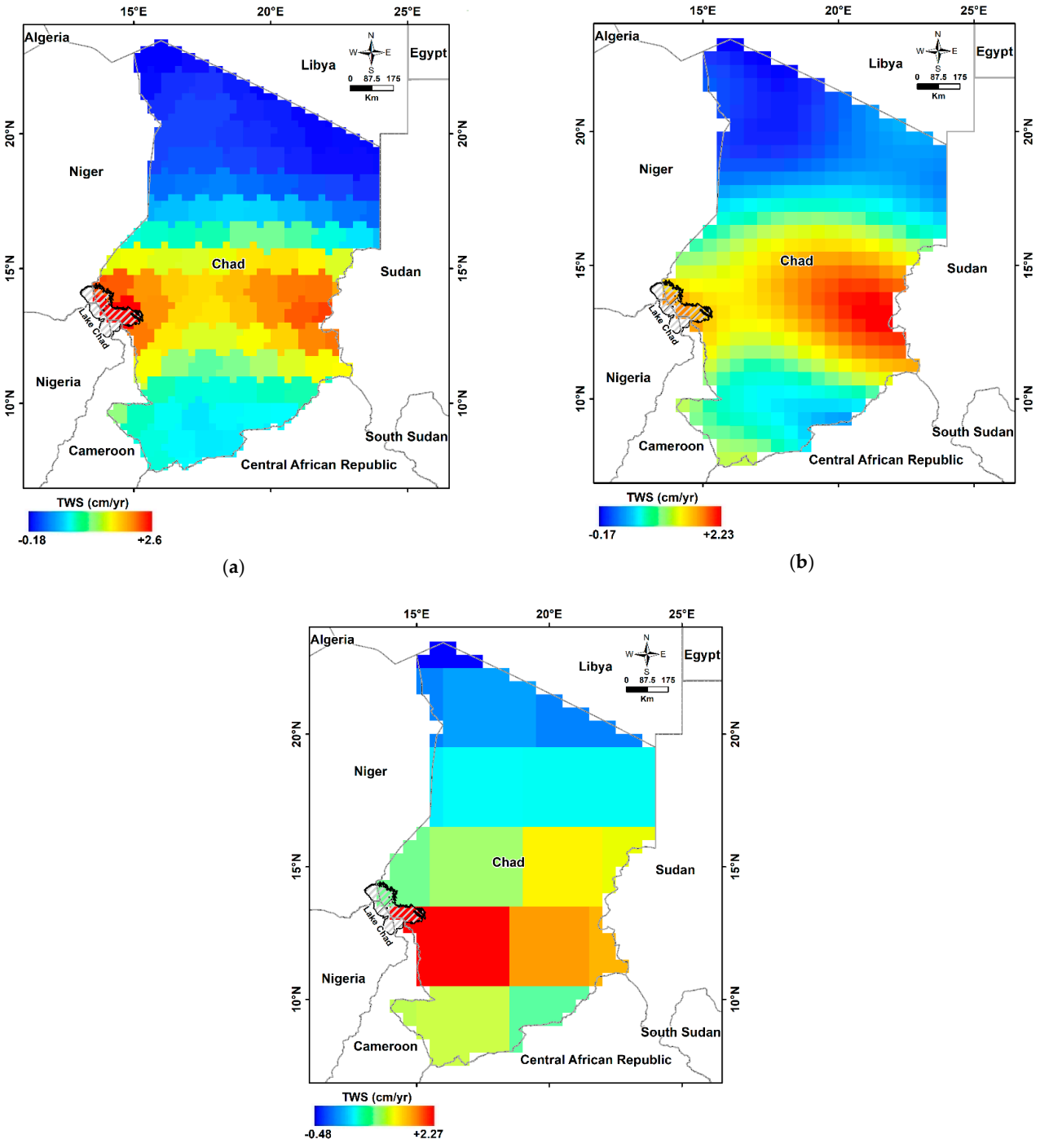

Figure 6. Spatiotemporal variation map of the ΔTWS trend during Period II from CSR (**a**), GSFC (**b**), and JPL (**c**) mascon products.

4.3. Examining the Lake Chad's Surface Water Levels over Time

The water level fluctuation in Lake Chad for the research period is displayed in Figure 9. Provided the increasing trend in precipitation during the entire period, the surface water level shows a slightly increasing trend of +3.05 ± 0.29 cm yr^{-1}. This compensates for a mass gain of +0.041 ± 0.004 km^3 yr^{-1} throughout the study period, given that the lake has a surface area of 1350 km^2. By averaging the mass gain (0.041 ± 0.004 km^3 yr^{-1}) of the

lake over the entire area (1,284,000 km^2), the regional increase rate was then calculated at +0.032 ± 0.003 mm yr$^{-1,}$ explaining about 0.012% of ΔTWS (Table 1).

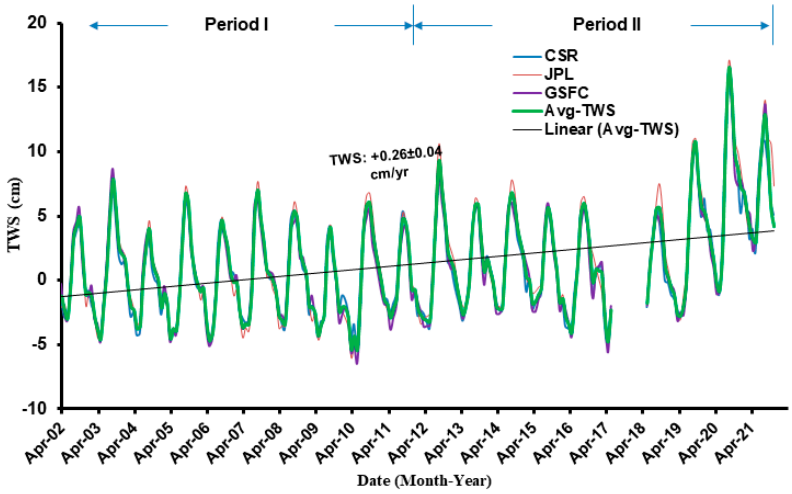

Figure 7. Monthly time series of the ΔTWS over Chad using the three mascon solutions and their mean.

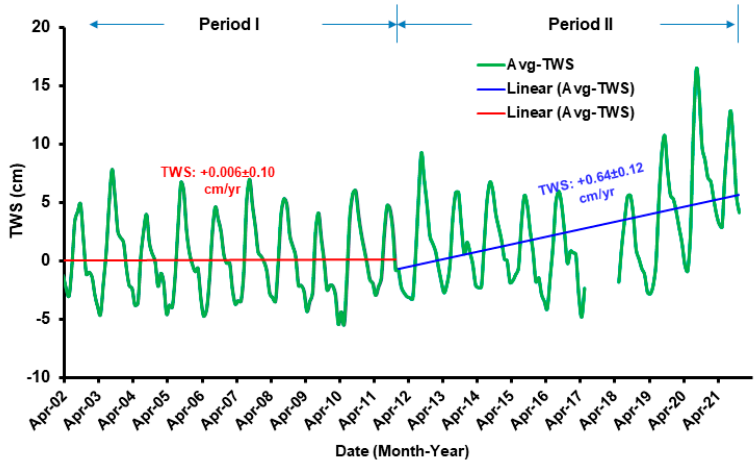

Figure 8. Shows the two periods' time series for the ΔTWS over Chad.

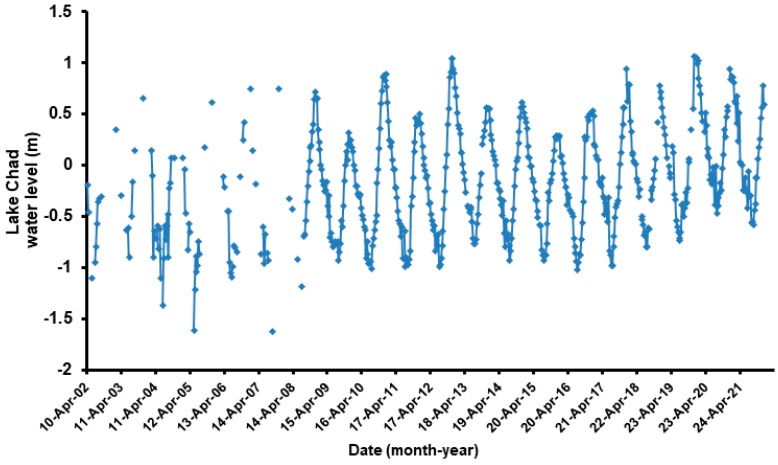

Figure 9. Displays a historical graph of Lake Chad's water level during the whole period.

The mass variation of the lake gained approximately +0.062 ± 0.013 km^3 yr^{-1} of water during Period I that is equal to +0.043 ± 0.01 mm yr^{-1} across the entire region, according

to piecewise linear trend analysis. During Period II, the volume of the water in the Lake increased to a rate of 0.038 ± 0.0 km^3 yr^{-1}, averaging at +0.030 ± 0.00 mm yr^{-1} over the entire study area.

4.4. Analysis of the ΔGWS

The temporal variations in the ΔGWS (Figure 10) show a similar pattern as those of ΔTWS with correlation coefficients varying from 0.95 to 0.98. The ΔGWS change (Figure 11) was estimated by subtracting the non-groundwater components represented by ΔSMS (Figure 11) from the TWS change using Equation (1). Changes in ΔCWS, ΔSWE and the surface runoff represent the other non-groundwater components that are negligible in this environment as no anomaly patterns were observed. An increase of +0.25 ± 0.04 cm yr^{-1} was calculated for the GWS (Figure 11; Table 1) during the whole period by the subtraction of the GLDAS-derived ΔSMS (+0.03 ± 0.02) and Lake Chad (+0.032 ± 0.003 mm yr^{-1}) trend values from the GRACE-estimated TWS trend (+0.26 ± 0.04 cm yr^{-1}). For Period I, the GLDAS-derived ΔSMS (0.016 ± 0.133 mm yr^{-1}) and Lake Chad (+0.043 ± 0.01 mm yr^{-1}) trend values were removed from the ΔTWS trend (+0.006 ± 0.10 cm yr^{-1}) to estimate the GWS at +0.0001 ± 0.099 cm yr^{-1} (Figure 11; Table 1). The ΔGWS change was estimated at +0.62 ± 0.12 cm yr^{-1} for Period II (Figure 11; Table 1) by subtracting the GLDAS-derived ΔSMS (+0.14 ± 0.13 mm yr^{-1}) and Lake Chad (+0.030 ± 0.00 mm yr^{-1}) trend values from the GRACE-derived TWS trend (+0.64 ± 0.12 cm yr^{-1}).

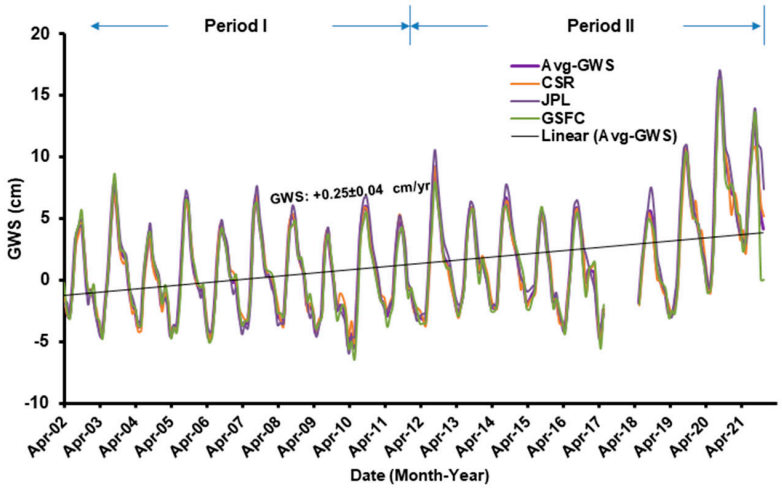

Figure 10. Monthly time series of the ΔGWS and their mean (Avg-GWS) using the three mascon solutions over Chad.

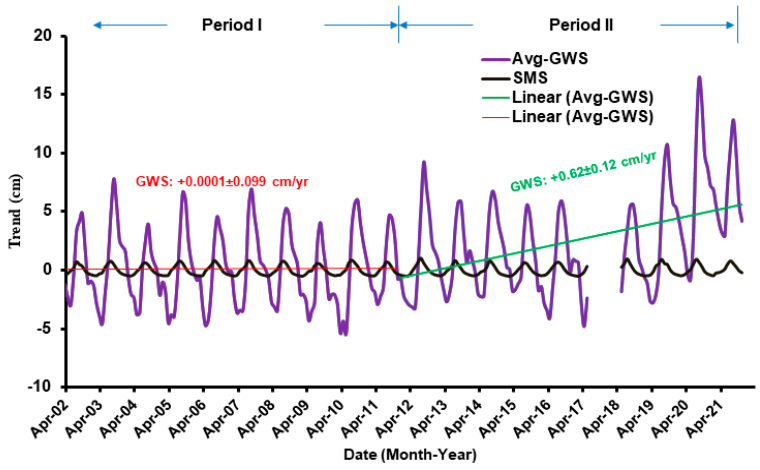

Figure 11. The Monthly ΔGWS and ΔSMS time series for the research region during the two periods.

The ΔGWS change shows an upward trend (+0.25 ± 0.04 cm yr^{-1}) during the entire period, which is about 0.96% of ΔTWS, and varying from a low value (+0.0001 ± 0.099 cm yr^{-1}) during Period I to a slightly higher value (+0.62 ± 0.12 cm yr^{-1}) throughout Period II. This increase is largely attributed to the increase in the precipitation rate, which shows an upward trend of 0.34 mm yr^{-1} during the whole period.

4.5. Recharge Rate

The substantial rainfall rate, and the lake Chad play important roles in recharging the groundwater aquifers. The natural recharge rate was estimated to be +4.11 ± 0.51 km^3 yr^{-1} (+0.32 ± 0.04 cm yr^{-1}; Table 1) for the investigated area during the entire period using Equation (2) by the addition of the mean annual groundwater pumping rate (0.88 ± 0.088 km^3 yr^{-1}, [69]) to the GRACE-derived GWS variation rate (+3.21 ± 0.51 km^3 yr^{-1}; Table 1).

$$\text{Recharge} = \Delta\text{GWS} + \text{Discharge} \quad (2)$$

Lower recharge rate was estimated to be +0.87 ± 1.27 km^3 yr^{-1} (+0.068 ± 0.099 cm yr^{-1}; Table 1) during Period I by the addition of the mean annual groundwater pumping rate (0.87 ± 0.087 km^3 yr^{-1}; [69]) to the ΔGWS rate (+0.001 ± 1.27 km^3 yr^{-1}). For Period II, a higher recharge rate of +8.86 ± 1.54 km^3 yr^{-1} (+0.69 ± 0.12 cm yr^{-1}; Table 1) was estimated for the study area by the addition of the yearly groundwater pumping values (0.88 ± 0.088 km^3 yr^{-1}; [69]) to the ΔGWS rate (+7.96 ± 1.54 km^3 yr^{-1}).

Chad's elevation map is depicted in Figure 12, which was created from the ETOPO1 Global Relief Model. Most of the country has ground surface levels ranging from about 100 m in the central eastern part, close to the border with Niger and increases toward the east and north, where it is reaching about 600 m at the foothills of the Tibesti, Erdi, Ennedi, and Darfur mountains. These mountains are referred to as the Southern Highlands, where they reach higher elevations up to 900 mm in Erdi and more than 3000 in the Tibesti mountains. The southern highlands are receiving a significant precipitation rate that formed surface streams (Figure 12). These streams take the water from the eastern and northern hilly regions to the lowlands in the central western part of the country. These streams may recharge the groundwater of the lowlands through the highly permeable surface sediments that are represented by aeolian sands, and fluviolacustrine sediments. The recharging of the upper aquifer zone in the southwestern region of the Chad Basin in Niger is largely evidenced by the presence of stable isotopic signatures (from −7‰ to +3‰ $\delta^{18}O$ and −50‰ to +14‰ δH), reflecting modern recharge from the rainfall at some places, where some of its waters have stable isotopic compositions that are comparable to the region's typical rainfall waters [70]. Another group of samples reflects mixing water between the rainfall and the water from Middle and Lower Zones confined aquifers. Ref. [71] (2010) used oxygen (^{18}O) and tritium (^{3}H) isotopes to analyze groundwater samples from the Lake Chad Basin's Quaternary aquifer. Their findings revealed an average annual renewal rate of 0.09%, or about 3 mm yr^{-1} of recharge, for a rainfall range of 250 to 550 mm. Groundwater bodies receive also indirect recharge from seepage through the beds of Lake Chad, Logone-Chari Rivers, local ponds, and non-permanent rivers (Komadugu Yobe). Another isotopic study has been carried out on the Chadian extent of the NSAS to locate the places of modern recharge [72]. Groundwater recharged by recent precipitation has stable isotopic values ($\delta^{18}O$: −6 to +6‰ and δH: −40 to −2‰) that are similar to the current precipitation over North and Central Africa as well as a distinctive Ca-Mg-(Na)-HCO^3 signature. This compositional group's geographic distribution closely resembles the pattern of heavier precipitation across the Ennedi and Tibesti mountains. The role of terrestrial water in the climate, weather, and biogeochemical cycles is crucial to the Earth system beyond its human and economic significance [73]. Therefore, knowing the internal dynamics of the TWS is not only necessary for human survival, but also for assessing the water cycle, policymaking, planning, and other strategies of management for water resources with a growing population [3,74,75].

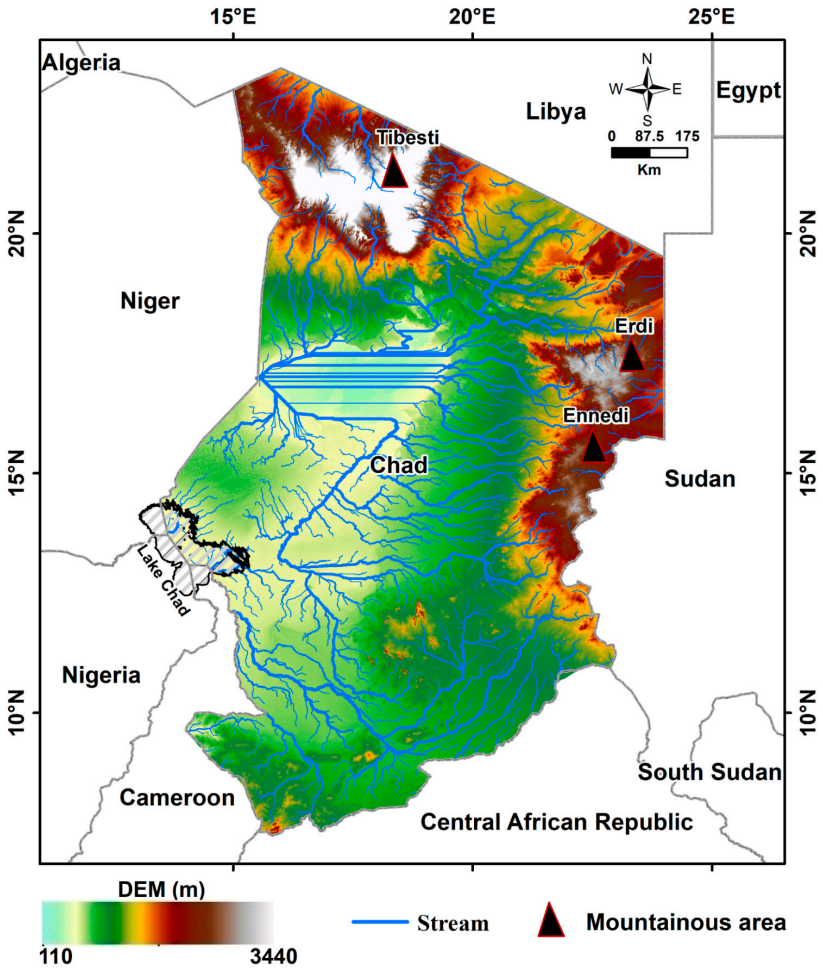

Figure 12. A map illustrating the local stream networks as well as the surface elevation of Chad using a digital elevation model (DEM).

4.6. Sediment Thickness

We have created a sediment thickness map for the research area using datasets from the NOAA's National Geophysical Data Center [76]. The sedimentary cover (Figure 13) increases, as can be seen, from 0 m at the mountainous highlands of Tibesti, Erdi, Ennedi, and Darfur to more than 2000 m at the northeastern part of the Kufra Basin, close to the border with Sudan and Libya. The thickness also increases towards the Lake Chad Basin, where it shows higher values up to 3000 m, close to the border with Niger as well as at the southern part of the country with values of more than 2000 m. The highly productive aquifers are found in the country's center and southern regions, with Lake Chad Basin constituting one of Africa's largest sedimentary basins for groundwater.

4.7. Structural Connection between the Kufra and the Dakhla Basins

The findings in this section are supported by some previously published studies ([31,77–82]; Figure 14). This figure depicts the distribution of the massive transcurrent faults of the Pelusium megashear system that runs through the Africa from the Mediterranean Sea to the eastern Nile delta [79]. It crosses Africa, curving southwest to the Niger River delta in Guinea. The southern Kufra Basin occupies the northwestern part of Sudan and the northeastern part of Chad. This region is receiving a substantial precipitation rate that occurs on the Tibesti, Erdi, Ennedi, and Darfur mountains that feed the southern Kufra Basin from the surface stream networks through the fractured rocks. The Kufra Basin is composed of high-thick shallow marine-fluvial deposits that date from the infracambrian to the Cretaceous [83]. The existence of these sediments suggests that larger groundwater

reserves have been accumulated. Despite its geological potential, the Kufra basin has received little attention due to its location at least 450 km from the nearest oil infrastructure (the Serir oilfield) and because AGIP drilled two unsuccessful wells there between 1978 and 1980. Siltstones have replaced the lower Silurian Tanezzuft shale, the main possible source rock interval, in these wells [84].

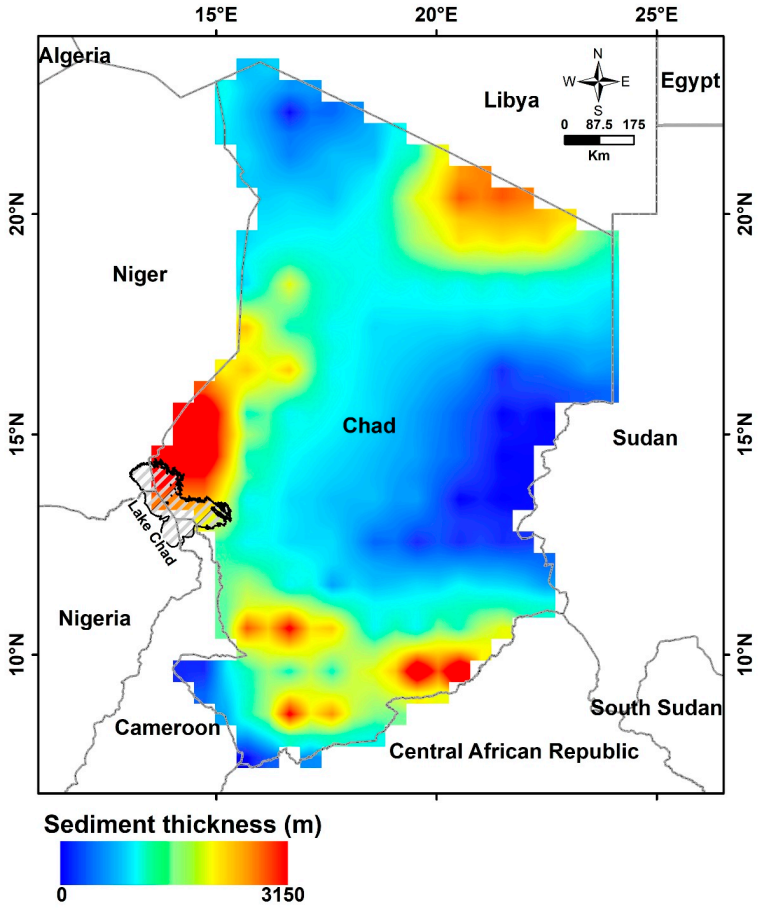

Figure 13. A representation of the sedimentary succession's thickness (m) in Chad.

Figure 14 shows also the southwest-to-northeast direction of the NSA's regional groundwater flow [77,78]. Such flow is largely parallel to the megashear system that may act as a preferred conduit for the groundwater flow from the Kufra Basin close to the Tibesti Mountains toward the Dakhla Basin in a northeasterly direction and to the Mediterranean Sea in a northerly direction [85]. Permeable sediment succession with a relatively higher hydraulic conductivity [86–88] inside and near the megashear facilitates groundwater movement to the northeast [31]. It appears that there is a groundwater flow pathway from Kufra and Sarir basins into the Dakhla Basin, as the groundwater ages steadily increase from Siwa to Qattara, and from northwest Farafra to north Bahariya Oasis [31,33]. In addition to cutting through the aquifer's sedimentary succession, this megashear reaches throughout the crust and uppermost mantle layer [33,81] based on the Helium isotopic ratio ($^3He/^4He$; [80]). The Lake Chad and the Kufra basins may be linked by the faults of the Pelusium megashear system, but additional research is needed to fully comprehend the hydraulic connection between the two basins. Groundwater flow from the Northern Sudan Platform to the Dakhla basin is obstructed by sectors of the EW-trending Uweinat–Aswan uplift [31]. This was evidenced by the isotopic data that has been made public and shows that oxygen and hydrogen are more abundant in the Northern Sudan platform than in the Dakhla Basin [31,89–92]. Krypton-81 and chlorine-36 suggest groundwater ages away from the uplift, with ages of 680×10^3 yr in Kharga and upto 1000×10^3 yr in the Bahariya [93,94].

The reported ages from regions south of the Uweinat-Aswan uplift contrast with these much older ages. Younger C-14 ages (50 × 10^3 yr) were documented from the northern Sudanese regions of Badr and Selima ([91]; Figure 14), as well as young Cl-36 ages at South Aswan (30 × 10^3 yr), and Abu Simbel (29–35 × 10^3 yr).

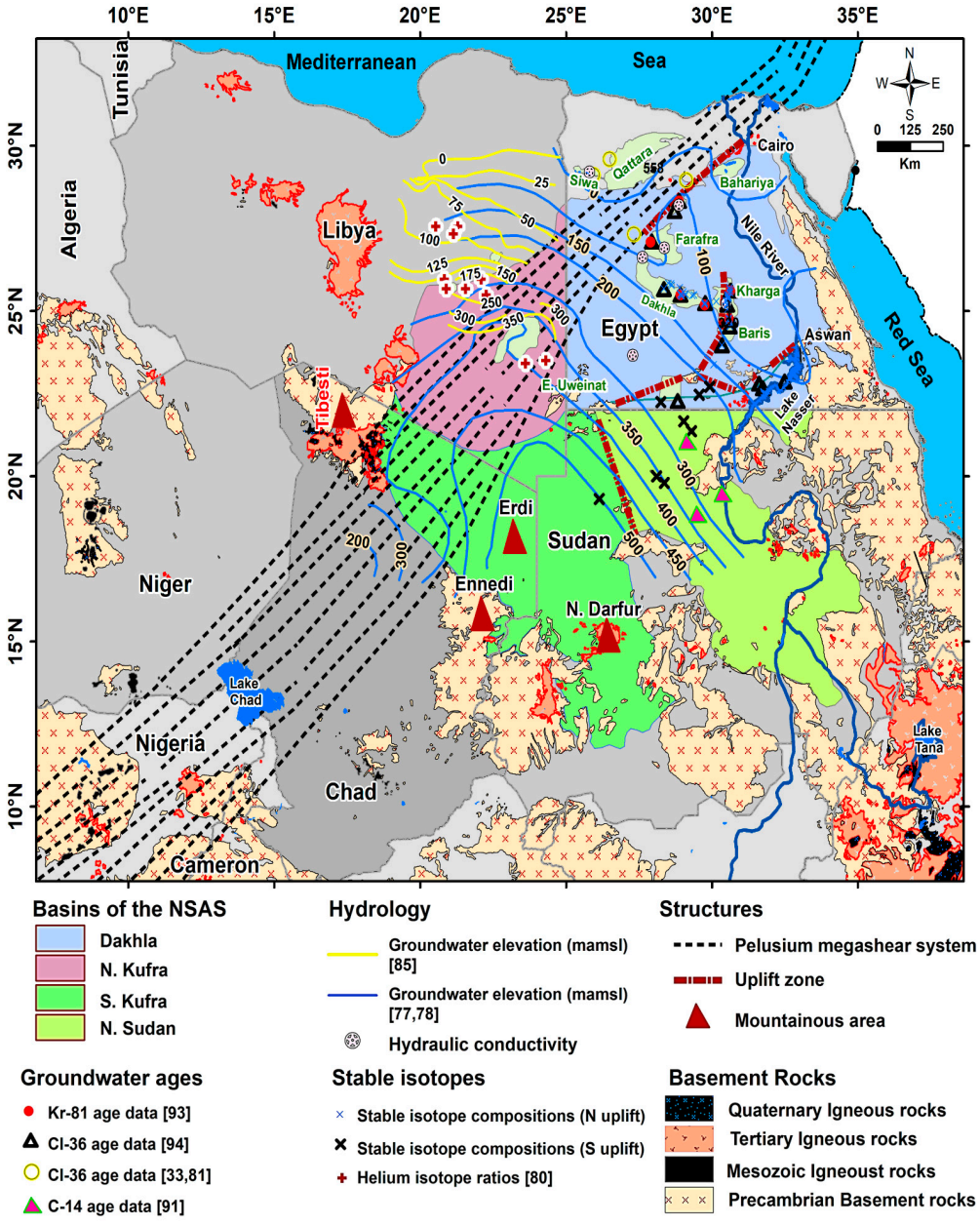

Figure 14. The distribution of the Pelusium megashear, the Uweinat-Aswan and Uweinat-Howar basement uplifts, the Kufra, Dakhla, and Northern Sudan Platform basins of the NSAS are all highlighted. Additionally, it shows the locations of groundwater samples that were located south and north of the Uweinat-Aswan uplift and were isotopically analysed (O, H) and dated (Kr-81; Cl-36; and C-14) in the aquifer.

4.8. Uncertainties, Implications, and Future Research

The GRACE total uncertainty was computed as the standard deviation of the calculated trends between various solutions [3,16,95]. The standard deviation was applied similarly to soil moisture, and surface water. In regions where glacial isostatic adjustment is considerable, errors in GRACE data are caused by spectral and spatial leakages, observations, post-processing, and glacial isostatic adjustment. A Student *t*-test was used

to examine the generated ΔGWS trend. The t-value and confidence chart are used to determine the probability (*p*-value) and statistically significant trends at the 95% level of confidence. At a *p*-value of 0.0001 for the ΔGWS trend, there is a significant upward trend at 95% confidence level. One-sigma trend errors in GWS were evaluated by propagating through various water storage components. All the variables in Equation (3) were obtained from other different sources with the exception of GWS.

$$\sigma_{GWS} = \sqrt{(\sigma_{TWS})^2 + (\sigma_{SMS})^2 + (\sigma_{SWS})^2} \quad (3)$$

Based on the errors found for TWS (σ_{TWS}), SMS (σ_{SMS}), and SWS (σ_{SWS}) in Table 1, the error (σ_{GWS}) in ΔGWS was calculated based on of Equation (3). The GRACE-derived ΔGWS trend between April 2002 and December 2021 is +0.25 cm/yr, with a corresponding error of 0.04 cm/yr.

Despite these unavoidable difficulties, the current work adds more to our understanding of groundwater variability in Chad for both current and future perspectives. According to the TWS and GWS estimates, central Chad has experienced the highest favorable TWS trend values (Figures 5 and 6), and the country as a whole has shown a water storage surplus, especially between 2012 and 2021 (Figures 7 and 10). This information could aid policymakers in increasing groundwater-dependent agricultural activities and community building. The groundwater storage plays a substantial role in TWS in Chad, and explains about 0.96% of TWS; hence, a continuous monitoring program utilizing the most recent GARCE data, meteorological models, and ground-based data should be carried out to assess the water storage dynamics in the future.

5. Conclusions

GRACE provides a novel method for determining variations in Chad's terrestrial water storage.

Our results show that groundwater storage in Chad has substantially improved from April 2002 to December 2021:

- Based on rainfall investigations in Chad, two different climatic periods spanning the research period were determined: Period I (April 2002 to December 2011) was witnessing a lower precipitation rate of 336.22 mm yr^{-1}; and following Period II (January 2012 to December 2021), which is receiving a higher rainfall rate of 377.8 mm yr^{-1}.
- During the entire study period, ΔTWS shows a broad improvement pattern.
- The increase rate of GWS for Period I was calculated at +0.0001 ± 0.099 cm yr^{-1}; and a higher rate of +0.62 ± 0.12 cm yr^{-1} was found for Period II.
- The GWS shows a cumulative increase rate of +0.25 ± 0.04 cm yr^{-1} throughout the investigated region over the entire examined period, which resulted from the higher rainfall rate prevailed over the study area.
- Surface waters from the surface streams running across the highlands of northern and central Chad replenish aquifers in locations with large sedimentary thicknesses.
- The higher rainfall rate over the southern region and Lake Chad is recharging the groundwater in those areas.
- The recharge rate was estimated to be +4.11 ± 0.51 km^3 yr^{-1} (0.32 ± 0.04 cm yr^{-1}) across the study region over the whole period.
- The Kufra Basin in northern Chad and southeastern Libya appears to be structurally connected to the Dakhla Basin along the structures of the Pelusium megashear system.
- We also demonstrated that GRACE, when combined with other relevant datasets, can be used to answer questions regarding where and how quickly recharge and discharge occur, whether groundwater reservoirs are at steady state or being recharged, and if being recharged, whether the recharge is the result of natural or anthropogenic processes.
- Answering the issues stated herein for Chad's groundwater resources is vital for optimum resource management and, more importantly, the development of repeatable concepts that can be easily applied to similar arid/semiarid regions around the world.

Author Contributions: Conceptualization, A.M. and A.A.; methodology, A.M. and A.A.; software, A.M.; validation, A.M., A.A., S.S.A. and A.O.; formal analysis, A.M. and A.A.; investigation, A.M.; resources, A.M., A.A., S.S.A. and A.O.; data curation, A.M. and A.A.; writing—original draft preparation, A.M. and A.A.; writing—review and editing, A.M.; visualization, A.M.; supervision, A.M. and A.O.; project administration, A.M. and A.A.; funding acquisition, S.S.A. All authors have read and agreed to the published version of the manuscript.

Funding: This research was funded by Researchers Supporting Project number (RSP2023R496), King Saud University, Riyadh, Saudi Arabia.

Data Availability Statement: The data is available upon request from the authors.

Acknowledgments: This research was supported by Researchers Supporting Project number (RSP2023R496), King Saud University, Riyadh, Saudi Arabia.

Conflicts of Interest: The authors declare no conflict of interest.

References

1. Rodell, M.; Famiglietti, J.S.; Wiese, D.N.; Reager, J.T.; Beaudoing, H.K.; Landerer, F.W.; Lo, M.H. Emerging trends in global freshwater availability. *Nature* **2018**, *557*, 651–659. [CrossRef] [PubMed]
2. Xiong, J.; Abhishek Guo, S.; Kinouchi, T. Leveraging machine learning methods to quantify 50 years of dwindling groundwater in India. *Sci. Total Environ.* **2022**, *835*, 155474. [CrossRef] [PubMed]
3. Abhishek Kinouchi, T.; Sayama, T. A comprehensive assessment of water storage dynamics and hydroclimatic extremes in the Chao Phraya River Basin during 2002–2020. *J. Hydrol.* **2021**, *603*, 126868. [CrossRef]
4. Van den Broeke, M.; Bamber, J.; Ettema, J.; Rignot, E.; Schrama, E.; van de Berg, W.J.; van Meijgaard, E.; Velicogna, I.; Wouters, B. Partitioning Recent Greenland Mass Loss. *Science* **2009**, *326*, 984–986. [CrossRef] [PubMed]
5. Abhishe; Kinouchi, T. Synergetic application of GRACE gravity data, global hydrological model, and in-situ observations to quantify water storage dynamics over Peninsular India during 2002–2017. *J. Hydrol.* **2021**, *596*, 126069. [CrossRef]
6. Pokhrel, Y.; Hanasaki, N.; Yeh, P.; Yeh, P.J.; Yamada, T.J.; Kanae, S.; Oki, T. Model estimates of sea-level change due to anthropogenic impacts on terrestrial water storage. *Nat. Geosci.* **2012**, *5*, 389–392. [CrossRef]
7. Ahmed, M. Sustainable management scenarios for northern Africa's fossil aquifer systems. *J. Hydrol.* **2020**, *589*, 125196. [CrossRef]
8. Skaskevych, A.; Lee, J.; Jung, H.; Bolten, J.; David, J.; Policelli, F.; Goni, I.; Favreau, G.; San, S.; Ichoku, C. Application of GRACE to the estimation of groundwater storage change in a data-poor region: A case study of Ngadda catchment in the Lake Chad Basin. *Hydrol. Process.* **2020**, *34*, 941–955. [CrossRef]
9. Postel, S. *Water in Crisis: A Guide to the World's Freshwater Resources*; Gleick, P.H., Ed.; Oxford University Press: Oxford, UK, 1993; pp. 56–66.
10. Rodell, M.; Velicogna, I.; Famiglietti, J.S. Satellite-based estimates of groundwater depletion in India. *Nature* **2009**, *460*, 999–1002. [CrossRef]
11. Purdy, A.J.; David, C.H.; Sikder, M.; Reager, J.T.; Chandanpurkar, H.A.; Jones, N.L.; Matin, M.A. An Open-Source Tool to Facilitate the processing of GRACE Observations and GLDAS outputs: An evaluation in Bangladesh. *Front. Environ. Sci.* **2019**, *7*, 155. [CrossRef]
12. Taylor, R.G.; Scanlon, B.; Döll, P.; Rodell, M.; Van Beek, R.; Wada, Y.; Longuevergne, L.; Leblanc, M.; Famiglietti, J.S.; Edmunds, M. Ground Water and Climate Change. *Nat. Clim. Chang.* **2013**, *3*, 322–329. [CrossRef]
13. Famiglietti, J.S. The Global Groundwater Crisis. *Nat. Clim. Chang.* **2014**, *4*, 945–948. [CrossRef]
14. McStraw, T.C.; Pulla, S.T.; Jones, N.L.; Williams, G.P.; David, C.H.; Nelson, J.E.; Ames, D.P. An Open-Source Web Application for the Processing of GRACE Observations and GLDAS Outputs: An Evaluation in Bangladesh. *Front. Environ. Sci.* **2021**, *7*, 155.
15. Famiglietti, J.S.; Rodell, M. Water in the Balance. *Science* **2013**, *340*, 1300–1301. [CrossRef]
16. Villholth, K.G. Groundwater Assessment and Management: Implications and Opportunities of Globalization. *Hydrogeol. J.* **2006**, *14*, 330–339. [CrossRef]
17. Scanlon, B.R.; Zhang, Z.; Save, H.; Sun, A.Y.; Schmied, H.M.; Van Beek, L.P.H.; Wiese, D.N.; Wada, Y.; Long, D.; Reedy, R.C.; et al. Global models underestimate large decadal declining and rising water storage trends relative to GRACE satellite data. *Proc. Natl. Acad. Sci. USA* **2018**, *115*, E1080–E1089. [CrossRef]
18. De Vries, J.J.; Simmers, I. Groundwater recharge: An overview of process and challenges. *Hydrogeol. J.* **2002**, *10*, 5–17. [CrossRef]
19. Milewski, A.; Sultan, M.; Yan, E.; Becker, R.; Abdeldayem, A.; Soliman, F.; Gelil, K.A. A remote sensing solution for estimating runoff and recharge in arid environments. *J. Hydrol.* **2009**, *373*, 1–14. [CrossRef]
20. Mohamed, A.; Ahmed, E.; Alshehri, F.; Abdelrady, A. The groundwater flow behavior and the recharge in the Nubian Sandstone Aquifer System during the wet and arid periods. *Sustainability* **2022**, *14*, 6823. [CrossRef]
21. Mohamed, A.; Asmoay, A.; Alshehri, F.; Abdelrady, A.; Othman, A. Hydro-geochemical applications and multivariate analysis to assess the water–rock interaction in arid environments. *Appl. Sci.* **2022**, *12*, 6340. [CrossRef]

22. Armanios, D.E.; Fisher, J.B. Measuring water availability with limited ground data: Assessing the feasibility of an entirely remotesensing-based hydrologic budget of the Rufiji Basin, Tanzania, using TRMM, GRACE, MODIS, SRB, and AIRS. *Hydrol. Process.* **2014**, *28*, 853–867. [CrossRef]
23. Becker, M.; Papa, F.; Frappart, F.; Alsdorf, D.; Calmant, S.; Santos da Silva, J.; Seyler, F. Satellite-based estimates of surface water dynamics in the Congo River Basin. *Int. J. Appl. Earth Obs. Geoinf.* **2018**, *66*, 196–209. [CrossRef]
24. Tapley, B.D.; Bettadpur, S.; Ries, J.C.; Thompson, P.F.; Watkins, M.M. GRACE measurements of mass variability in the Earth system. *Science* **2004**, *305*, 503–505. [CrossRef]
25. Schmidt, R.; Schwintzer, P.; Flechtner, F.; Reigber, C.; Güntner, A.; Döll, P.; Ramillien, G.; Cazenave, A.; Petrovic, S.; Jochmann, H.; et al. GRACE observations of changes in continental water storage. *Glob. Planet Chang.* **2006**, *50*, 112–126. [CrossRef]
26. Rodell, M.; Chen, J.; Kato, H.; Famiglietti, J.S.; Nigro, J.; Wilson, C.R. Estimating groundwater storage changes in the Mississippi River basin (USA) using GRACE. *Hydrogeol. J.* **2007**, *15*, 159–166. [CrossRef]
27. Swenson, S.; Wahr, J. Post-processing removal of correlated errors in GRACE data. *Geophys. Res. Lett.* **2006**, *3*, L08402. [CrossRef]
28. Zhang, Y.; Yao, L.; Jing, G.; Gaopeng, L.; Zhisheng, Y.; Haishan, N. Correlation analysis between drought indices and terrestrial water storage from 2002 to 2015 in China. *Environ. Earth Sci.* **2018**, *77*, 462. [CrossRef]
29. Voss, K.A.; Famiglietti, J.S.; Lo, M.; De Linage, C.; Rodell, M.; Swenson, S.C. Groundwater depletion in the Middle East from GRACE with implications for transboundary water management in the Tigris–Euphrates–western Iran region. *Water Resour. Res.* **2013**, *49*, 904–914. [CrossRef]
30. Alshehri, F.; Mohamed, A. Analysis of Groundwater Storage Fluctuations Using GRACE and Remote Sensing Data in Wadi As-Sirhan, Northern Saudi Arabia. *Water* **2023**, *15*, 282. [CrossRef]
31. Mohamed, A.; Sultan, M.; Ahmed, M.; Yan, E.; Ahmed, E. Aquifer recharge, depletion, and connectivity: Inferences from GRACE, land surface models, and geochemical and geophysical data. *Bull. Geol. Soc. Am.* **2017**, *129*, 534–546. [CrossRef]
32. Taha, A.I.; Al Deep, M.; Mohamed, A. Investigation of groundwater occurrence using gravity and electrical resistivity methods: A case study from Wadi Sar, Hijaz Mountains, Saudi Arabia. *Arab. J. Geosci.* **2021**, *14*, 334. [CrossRef]
33. Mohamed, A. Hydro-geophysical study of the groundwater storage variations over the Libyan area and its connection to the Dakhla basin in Egypt. *J. Afr. Earth Sci.* **2019**, *157*, 103508. [CrossRef]
34. Mohamed, A. Gravity based estimates of modern recharge of the Sudanese area. *J. Afr. Earth Sci.* **2020**, *163*, 103740. [CrossRef]
35. Mohamed, A. Gravity applications in estimating the mass variations in the Middle East: A case study from Iran. *Arab. J. Geosci.* **2020**, *13*, 364. [CrossRef]
36. Mohamed, A. Gravity applications to groundwater storage variations of the Nile Delta Aquifer. *J. Appl. Geophys.* **2020**, *182*, 104177. [CrossRef]
37. Mohamed, A.; Gonçalvès, J. Hydro-geophysical monitoring of the North Western Sahara Aquifer System's groundwater resources using gravity data. *J. Afr. Earth Sci.* **2021**, *178*, 104188. [CrossRef]
38. Mohamed, A.; Ragaa Eldeen, E.; Abdelmalik, K. Gravity based assessment of spatio-temporal mass variations of the groundwater resources in the Eastern Desert, Egypt. *Arab. J. Geosci.* **2021**, *14*, 500. [CrossRef]
39. Mohamed, A.; Faye, C.; Othman, A.; Abdelrady, A. Hydro-geophysical Evaluation of the Regional Variability of Senegal's Terrestrial Water Storage Using Time-Variable Gravity Data. *Remote Sens.* **2022**, *14*, 4059. [CrossRef]
40. Mohamed, A.; Abdelrahman, K.; Abdelrady, A. Application of Time-Variable Gravity to Groundwater Storage Fluctuations in Saudi Arabia. *Front. Earth Sci.* **2022**, *10*, 873352. [CrossRef]
41. Mohamed, A.; Al Deep, M.; Othman, A.; Taha, A.L.; Alshehri, F.; Abdelrady, A. Integrated Geophysical Assessment of groundwater potential in southwestern Saudi Arabia. *Front. Earth Sci.* **2022**, *10*, 937402. [CrossRef]
42. Othman, A.; Abdelrady, A.; Mohamed, A. Monitoring Mass Variations in Iraq Using Time-Variable Gravity Data. *Remote Sens.* **2022**, *14*, 3346. [CrossRef]
43. Rodell, M.; Famiglietti, J.S. The potential for satellite-based monitoring of groundwater storage changes using GRACE: The high plains aquifer, central U.S. *J. Hydrol.* **2002**, *263*, 245–256. [CrossRef]
44. Rodell, M.; Famiglietti, J.S.; Chen, J.; Seneviratne, S.I.; Viterbo, P.; Holl, S.; Wilson, C.R. Basin scale estimates of evapotranspiration using GRACE and other observations. *Geophys. Res. Lett.* **2004**, *31*, L20504. [CrossRef]
45. Moiwo, J.; Tao, F.; Lu, W. Estimating soil moisture storage change using quasiterrestrial water balance method. *Fuel Energy Abstr.* **2011**, *102*, 25–34.
46. GWP (Global Water Partnership). *The Lake Chad Basin Aquifer System. Global Water Partnership Transboundary Groundwater Fact Sheet, Compiled by F Bontemps*; GWP (Global Water Partnership): Stockholm, Sweden, 2013.
47. United Nations. *Chad: In Groundwater in North and West Africa*; Natural Resources/Water Series No. 18, ST/TCD/5; United Nations Department of Technical Cooperation for Development and Economic Commission for Africa: Addis Ababa, Ethiopia, 1988.
48. Mohamed, A.; Al Deep, M. Depth to the bottom of the magnetic layer, crustal thickness, and heat flow in Africa: Inferences from gravity and magnetic data. *J. Afr. Earth Sci.* **2021**, *179*, 104204. [CrossRef]
49. Mohamed, A.; Abdelrady, M.; Alshehri, F.; Mohammed, M.A.; Abdelrady, A. Detection of Mineralization Zones Using Aeromagnetic Data. *Appl. Sci.* **2022**, *12*, 9078. [CrossRef]
50. Al Deep, M.; Araffa, S.A.S.; Mansour, S.A.; Taha, A.I.; Mohamed, A.; Othman, A. Geophysics and remote sensing applications for groundwater exploration in fractured basement: A case study from Abha Area, Saudi Arabia. *J. Afr. Earth Sci.* **2021**, *184*, 04368. [CrossRef]

51. Mohamed, A.; Al Deep, M.; Abdelrahman, K.; Abdelrady, A. Geometry of the magma chamber and curie point depth beneath Hawaii Island: Inferences from magnetic and gravity data. *Front. Earth Sci.* **2022**, *10*, 847984. [CrossRef]
52. Othman, A. Measuring and Monitoring Land Subsidence and Earth Fissures in Al-Qassim Region, Saudi Arabia: Inferences from InSAR. In *Advances in Remote Sensing and Geo Informatics Applications, Proceedings of the Conference of the Arabian Journal of Geosciences, CAJG 2018, Hammamet, Tunisia, 12–15 November 2018*; El-Askary, H., Lee, S., Heggy, E., Pradhan, B., Eds.; Advances in Science, Technology & Innovation (IEREK Interdisciplinary Series for Sustainable Development); Springer: Cham, Switzerland, 2019.
53. Goni, I.B. Estimating Groundwater Recharge in the Southwestern Sector of the Chad Basin Using Chloride Data. In *Applied Groundwater Studies in Africa*; Selected Papers in Hydrogeology, No 13, IAH; Mac Donald, A., Ed.; CRC Press: Boca Raton, FL, USA, 2008; pp. 323–336.
54. Luthcke, S.B.; Sabaka, T.J.; Loomis, B.D.; Arendt, A.A.; McCarthy, J.J.; Camp, J. Antarctica, Greenland and Gulf of Alaska land-ice evolution from an iterated GRACE global mascon solution. *J Glaciol.* **2013**, *59*, 613–631. [CrossRef]
55. Watkins, M.; Flechtner, F.; Webb, F. In Proceedings of the GRACE Science Team Meeting, Austin, TX, USA, 20–22 September 2015. Available online: https://www2.csr.utexas.edu/grace/GSTM/2015/proceedings.html (accessed on 7 December 2022).
56. Wiese, D.N.; Landerer, F.W.; Watkins, M.M. Quantifying and reducing leakage errors in the JPL RL05M GRACE mascon solution. *Water Resour. Res.* **2016**, *52*, 7490–7502. [CrossRef]
57. Save, H.; Bettadpur, S.; Tapley, D.D. High resolution CSR GRACE RL05 mascons. *J. Geophys. Res. Solid Earth* **2016**, *121*, 7547–7569. [CrossRef]
58. Save, H. CSR GRACE and GRACE-FO RL06 Mascon Solutions v02. Mascon Solut. *JCR Solid Earth* **2020**, *12*, 24. Available online: https://sealevel.nasa.gov/data/dataset/?identifier=SLCP_CSR-RL06-Mascons-v02_RL06_v02 (accessed on 7 December 2022).
59. Loomis, B.D.; Luthcke, S.B.; Sabaka, T.J. Regularization and error characterization of GRACE mascons. *J. Geod.* **2019**, *93*, 1381–1398. [CrossRef] [PubMed]
60. Sakumura, C.; Bettadpur, S.; Bruinsma, S. Ensemble Prediction and Intercomparing Analysis of GRACE Time-Variable Gravity Field Models. *Geophys. Res. Lett.* **2014**, *41*, 1389–1397. [CrossRef]
61. Tiwari, V.M.; Wahr, J.; Swenson, S. Dwindling groundwater resources in northern India, from satellite gravity observations. *Geophys. Res. Lett.* **2009**, *36*, L18401. [CrossRef]
62. Chen, J.; Famigliett, J.S.; Scanlon, B.R.; Rodell, M. Groundwater Storage Changes: Present Status from GRACE Observations. *Surv. Geophys.* **2016**, *37*, 397–417. [CrossRef]
63. G-REALM—Home. Available online: https://ipad.fas.usda.gov/cropexplorer/global_reservoir (accessed on 7 December 2022).
64. Kummerow, C. Beamfilling errors in passive microwave rainfall retrievals. *J. Appl. Meteorol.* **1998**, *37*, 356–370. [CrossRef]
65. Huffman, G.J.; Bolvin, D.T.; Nelkin, E.J.; Wolff, D.B.; Adler, R.F.; Gu, G.; Hong, Y.; Bowman, K.P.; Stocker, E.F. The TRMM Multisatellite Precipitation Analysis (TMPA): Quasi-global, multiyear, combined-sensor precipitation estimates at fine scales. *J. Hydrometeorol.* **2007**, *8*, 38–55. [CrossRef]
66. Cheema, M.J.M.; Bastiaanssen, W.G.M. Local calibration of remotely sensed rainfall from the TRMM satellite for different periods and spatial scales in the Indus Basin. *Int. J. Remote Sens.* **2012**, *33*, 2603–2627. [CrossRef]
67. Buma, W.G.; Lee, S.-I.; Seo, J.Y. Hydrological evaluation of Lake Chad Basin using space borne and hydrological model observation. *Water* **2016**, *8*, 205. [CrossRef]
68. Goncalves, J.; Petersen, J.; Deschamps, P.; Hamelin, B.; Baba-Sy, O. Quantifying the modern recharge of the "fossil" Sahara aquifers. *Geophys. Res. Lett.* **2013**, *40*, 2673–2678. [CrossRef]
69. FAO. AQUASTAT Website. Food and Agriculture Organization of the United Nations. 2022. Available online: http://www.fao.org/statistics/fr/ (accessed on 10 July 2022).
70. Goni, I.B. Tracing stable isotope values from meteoric water to groundwater in the southwestern part of the Chad basin. *Hydrogeol. J.* **2006**, *14*, 742–752. [CrossRef]
71. Oursingbé, M.; Zhonghua, T. Recharge of the Quaternary Aquifer of Lake Chad Basin Estimated from Oxygen-18 (18O) and Tritium (3H) Isotopes. *J. Am. Sci.* **2010**, *6*, 283–292.
72. Marie-Louise, V.; Sebastian, P.; Abderamane, H.; Francois, Z.; Daniel, H.; Philip, B. 20th EGU General Assembly, EGU2018. In Proceedings of the Conference, Vienna, Austria, 4–13 April 2018; p. 19407.
73. Seyoum, W.M.; Milewski, A.M. Improved methods for estimating local terrestrial water dynamics from GRACE in the Northern High Plains. *Adv. Water Resour.* **2017**, *110*, 279–290. [CrossRef]
74. Papa, F.; Frappart, F.; Malbeteau, Y.; Shamsudduha, M.; Vuruputur, V.; Sekhar, M.; Ramillien, G.; Prigentm, C.; Aires, F.; Clamant, S. Satellite-derived surface and sub-surface water storage in the Ganges–Brahmaputra River Basin. *J. Hydrol.* **2015**, *4*, 15–35. [CrossRef]
75. Wada, Y.; Wisser, D.; Bierkens, M.F.P. Global modeling of withdrawal, allocation and consumptive use of surface water and groundwater resources. *Earth Syst. Dyn.* **2014**, *5*, 15–40. [CrossRef]
76. Divins, D. *Total Sediment Thickness of the World's Oceans and Marginal Seas*; NOAA National Geophysical Data Center: Boulder, CO, USA, 2003.
77. Ball, J. Problems of the Libyan desert. *Geogr. J.* **1927**, *70*, 21–38. [CrossRef]
78. Sandford, K.S. Sources of Water in the North-Western Sudan. *Source: Geogr. J.* **1935**, *85*, 412–431. Available online: http://www.jstor.org/stable/1785619 (accessed on 7 December 2022). [CrossRef]

79. Neev, D.; Hall, J.K.; Saul, J.M. The Pelusium megashear system Across Africa and associated lineament swarms. *J. Geophys. Res.* **1982**, *87*, 1015–1030. [CrossRef]
80. Al Faitouri, M. Isotope and Noble Gas Study of Three Aquifers in Central and Eastern Libya. Ph.D. Thesis, Colorado State University, Fort Collins, CO, USA, 2013.
81. Mohamed, A. Constraints on the Amount and Passages of Groundwater Flow in the Nubian Sandstone Aquifer across Political Boundaries, Egypt. Ph.D. Thesis, Faculty of Science, Assiut University, Asyut, Egypt, 2016; p. 197.
82. Mohamed, A.; Sultan, M.; Yan, E.; Ahmed, E.; Sturchio, N.C. Towards a Better Understanding of the Hydrologic Setting of the Nubian Sandstone Aquifer System: Inferences from Groundwater Flow Models, CL-36 Ages, and GRACE Data. In Proceedings of the AGU Fall Meeting Abstracts, San Francisco, CA, USA, 14–18 December 2015.
83. Lüning, S.; Craig, J.; Fitches, B.; Mayouf, J.; Busrewil, A.; El Dieb, M.; Gammudi, A.; Loydell, D.K. *Chapter 8—Petroleum Source and Reservoir Rock Re-Evaluation in the Kufra Basin (SE Libya, NE Chad, NW Sudan)*; Geological Exploration in Murzuq Basin; Sola, M.A., Worsley, D., Eds.; Elsevier Science: Amsterdam, The Netherlands, 2000; pp. 151–173; ISBN 9780444506115. [CrossRef]
84. Bellini, E.; Giori, I.; Ashuri, O.; Benelli, F. Geology of Al Kufrah Basin, Libya. In *The Geology of Libya*; Salem, M.J., Sbeta, A.M., Bakbak, M.R., Eds.; Elsevier: Amsterdam, The Netherlands, 1991; Volume 6, pp. 2155–2184.
85. Wright, E.P.; Benfield, A.C.; Edmunds, W.M.; Kitching, R. Hydrogeology of the Kufra and Sirte Basins, Eastern Libya. *Q. J. Eng. Geol. Hydrogeol.* **1982**, *15*, 83–103. [CrossRef]
86. Thorweihe, U. Hydrogeologie des Dakhla Beckens (Ägypten): Berliner Geowissenschaftliche Abhandlungen. *Ser. A* **1982**, *38*, 1–58.
87. El Ramly, L. *Water Resources Study of Zone V—Al Kufra and Sirte Basins, Socialist Peoples' Libyan Arab Jamahiriya*; Technical Report; Secretariat of Agricultural Reclamation and Land Development: Tripoli, Libya, 1983; 136p, appendices.
88. CEDARE. *Regional Strategy for the Utilization of the Nubian Sandstone Aquifer System-Hydrogeology*; Centre for the Environment and Development for the Arab Region and Europe: Cairo, Egypt, 2001.
89. Haynes, C.V.; Haas, H. Radiocarbon evidence for Holocene recharge of groundwater, Western Desert, Egypt. *Radiocarbon* **1980**, *22*, 705–717. [CrossRef]
90. Hesse, K.-H.; Hissene, A.; Kheir, O.; Schnaecker, E.; Schneider, M.; Thorweihe, U. Hydrogeological investigations of the Nubian Aquifer System, Eastern Sahara. *Berl. Geowiss. Abh. Ser. A* **1987**, *75*, 397–464.
91. Froehlich, K.; Aggarwal, P.K.; Garner, W.A. An Integrated Approach in Evaluating Isotope Data of the Nubian Sandstone Aquifer System (NSAS) in Egypt (IAEA-CN-151/147). In *Proceedings, Advances in Isotope Hydrology and Its Role in Sustainable Water Resources Management (IHS-2007)*; International Atomic Energy Agency (IAEA): Vienna, Austria, 2007; Volume 1, pp. 31–45.
92. Sultan, M.; Ahmed, M.; Sturchio, N.; Eugene, Y.; Milewski, A.; Becker, R.; Wahr, J.; Becker, D.; Chouinard, K. Assessment of the vulnerabilities of the Nubian Nubian Sandstone Fossil Aquifer, North Africa. In *Climate Vulnerability: Understanding and Addressing Threats to Essential Resources: Amsterdam*; Pielke, R.A., Ed.; Elsevier: Amsterdam, The Netherlands, 2013; Volume 5, pp. 311–333. [CrossRef]
93. Sturchio, N.C.; Du, X.; Purtschert, R.; Lehmann, B.E.; Sultan, M.; Patterson, L.J.; Lu, Z.-T.; Müller, P.; Bigler, T.; Bailey, K.; et al. One million year old groundwater in the Sahara revealed by krypton-81 and chlorine-36. *Geophys. Res. Lett.* **2004**, *31*, L05503. [CrossRef]
94. Patterson, L.J.; Sturchio, N.C.; Kennedy, B.M.; van Soest, M.C.; Sultan, M.; Lu, Z.-T.; Lehmann, B.; Purtschert, R.; El Alfy, Z.; El Kaliouby, B.; et al. Cosmogenic, radiogenic, and stable isotopic constraints on groundwater residence time in the Nubian Aquifer, Western Desert of Egypt: Geochemistry, Geophysics. *Geosystems* **2005**, *6*, Q01005. [CrossRef]
95. Li, B.; Rodell, M.; Kumar, S.; Beaudoing, H.K.; Getirana, A.; Zaitchik, B.F.; de Goncalves, L.G.; Cossetin, C.; Bhanja, S.; Mukherjee, A.; et al. Global GRACE Data Assimilation for Groundwater and Drought Monitoring: Advances and Challenges. *Water Resour. Res.* **2019**, *55*, 7564–7586. [CrossRef]